AD-A118 924 ILLINOIS UNIV AT URBANA ELECTROMAGNETICS LAB F/G 9/5
ANALYSIS OF DOMINANT AND HIGHER-ORDER MODES IN UNILATERAL FIN L--ETC(U)
AUG 82 Y HAYASHI, E FARR, R MITTRA DAAG29-82-K-0084
UNCLASSIFIED UIEM-82-9 ARO-18094.3-EL NL

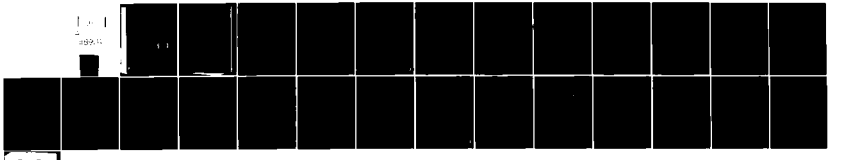

END
DATE FILMED
10 82
DTIC

ARO 18054.3-EL

(12)

ANALYSIS OF DOMINANT AND HIGHER-ORDER MODES IN UNILATERAL FIN LINES

INTERIM TECHNICAL REPORT

Y. HAYASHI*

E. FARR

R. MITTRA

AUGUST 1982

U. S. ARMY RESEARCH OFFICE

CONTRACT NO. DAAG29-82-K-0084

ELECTROMAGNETICS LABORATORY
DEPARTMENT OF ELECTRICAL ENGINEERING
ENGINEERING EXPERIMENT STATION
UNIVERSITY OF ILLINOIS AT URBANA-CHAMPAIGN
URBANA, ILLINOIS 61801

*Kitami Institute of Technology
Koen-cho, Kitami-shi, Hokkaido, 090 JAPAN.

THE FINDINGS IN THIS REPORT ARE NOT TO BE CONSTRUED AS AN OFFICIAL DEPARTMENT OF THE ARMY POSITION, UNLESS SO DESIGNATED BY OTHER AUTHORIZED DOCUMENTS.

UNCLASSIFIED

SECURITY CLASSIFICATION OF THIS PAGE (When Data Entered)

REPORT DOCUMENTATION PAGE		READ INSTRUCTIONS BEFORE COMPLETING FORM
1. REPORT NUMBER	2. GOVT ACCESSION NO.	3. RECIPIENT'S CATALOG NUMBER
4. TITLE (and Subtitle) ANALYSIS OF DOMINANT AND HIGHER-ORDER MODES IN UNILATERAL FIN LINES		5. TYPE OF REPORT & PERIOD COVERED Interim Technical Report
		6. PERFORMING ORG. REPORT NUMBER EM 82-9; UILU-ENG-82-2548
7. AUTHOR(s) Y. Hayashi*, E. Farr, and R. Mittra *Kitami Institute of Technology, Koen-cho, Kitami-shi, Hokkaido, 090 JAPAN.		8. CONTRACT OR GRANT NUMBER(s) DAAG29-82-K-0084
9. PERFORMING ORGANIZATION NAME AND ADDRESS Electromagnetics Laboratory Department of Electrical Engineering University of Illinois, Urbana, IL 61801		10. PROGRAM ELEMENT, PROJECT, TASK AREA & WORK UNIT NUMBERS P 18054-EL
11. CONTROLLING OFFICE NAME AND ADDRESS U. S. Army Research Office P. O. Box 12211 Research Triangle Park, N.C. 27709		12. REPORT DATE August 1982 13. NUMBER OF PAGES 24
14. MONITORING AGENCY NAME & ADDRESS(if different from Controlling Office)		15. SECURITY CLASS. (of this report) UNCLASSIFIED 15a. DECLASSIFICATION/ DOWNGRADING SCHEDULE

16. DISTRIBUTION STATEMENT (of this Report)

Distribution Unlimited.
Approved for public release.

17. DISTRIBUTION STATEMENT (of the abstract entered in Block 20, if different from Report)

18. SUPPLEMENTARY NOTES

The findings in this report are not to be construed as an official Department of the Army position, unless so designated by other authorized documents.

19. KEY WORDS (Continue on reverse side if necessary and identify by block number)

Millimeter Waves; Transmission Lines; Fin Lines; Dominant and Higher-Order Modes

20. ABSTRACT (Continue on reverse side if necessary and identify by block number)

In this paper, an analysis of dominant and higher-order modes in unilateral fin lines is presented. The network analysis method of electromagnetic fields is used along with Galerkin's method to obtain a determinantal equation. Numerical results are presented.

DD FORM 1 JAN 73 1473 EDITION OF 1 NOV 65 IS OBSOLETE

UNCLASSIFIED

SECURITY CLASSIFICATION OF THIS PAGE (When Data Entered)

UILU-ENG-82-2548

Electromagnetics Laboratory Report No. 82-9

ANALYSIS OF DOMINANT AND HIGHER-ORDER MODES IN UNILATERAL FIN LINES

by

Y. Hayashi*
E. Farr
R. Mittra

Electromagnetics Laboratory
Department of Electrical Engineering
University of Illinois at Urbana-Champaign
Urbana, Illinois 61801

*Kitami Institute of Technology,
Koen-cho, Kitami-shi, Hokkaido, 090 JAPAN.

Interim Technical Report

August 1982

Partially supported by

U. S. Army Research Office
Contract No. DAAG29-82-K-0084

TABLE OF CONTENTS

LIST OF FIGURES

Introduction

In recent years, fin line structures have become increasingly more attractive for millimeter-wave integrated circuit components. This has occurred because fin lines are low loss at millimeter-wave frequencies, and they are easily built using printed circuit techniques. The initial structure to be analyzed is shown in Figure 1. While the theory developed is general for three layers of dielectric, numerical results are presented for a single layer of dielectric, i.e., d=s=0.

This structure was also analyzed by Knoor and Shayda [1]. Their paper used the following approximation for the aperture field

$$e_x = \begin{cases} 0 & |x| \leq W \\ 1 & \text{elsewhere} \end{cases}$$
$$e_y = 0 \qquad (1)$$

In our analysis, the aperture fields are expressed in a more general form by expanding them in a series of basis functions, so the solution is believed to be more accurate. Also, higher-order mode characteristics are analyzed in this paper whereas only the dominant mode characteristic was presented in reference [1]. This allows us to study the range of single-mode operation and the characteristics of overmoding in these guides.

Determinantal Equation

In reviewing the published literature one finds that various fin line structures have been analyzed using spectral domain techniques [2] and [3]. On the other hand, the network analytical methods of electromagnetic fields [4] have been applied to the analysis of slot lines. These two methods represent the same approach in that they are based on Galerkin's method and

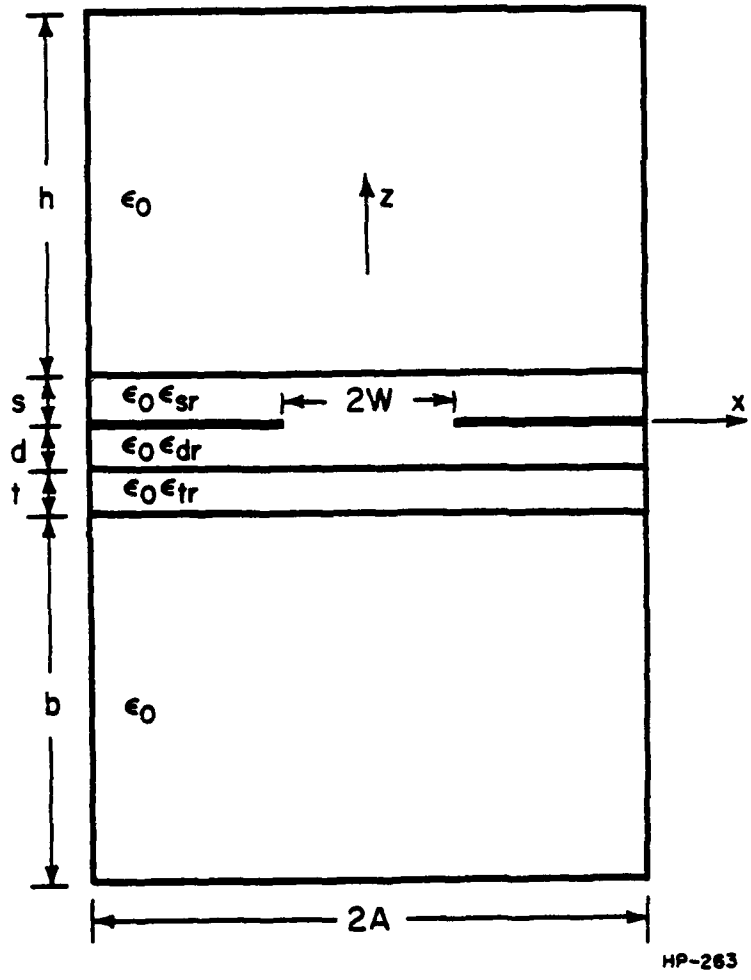

Figure 1. Cross-sectional view of unilateral fin line with three dielectric slabs. Here, ϵ_r = 2.2, h = 0.094", b = 0.089", t = 0.005", d = 0, s = 0, W = 0.0235", A = 0.047", and W/A = 0.5. The outer rectangular waveguide is WR-19, which has a cutoff frequency of 31.40 GHz.

Fourier transformations, and they ultimately lead to the same determinantal equation to be solved. Only the key steps are given here in order to avoid repetition of reference [4].

We begin with the spectral representation of the transverse electric and magnetic fields

$$\left.\begin{matrix} E_t \\ H_t \end{matrix}\right\} = \frac{1}{\sqrt{2\pi}} \int_{-\infty}^{\infty} \sum_{m=0}^{\infty} \sum_{\ell=1}^{2} \left\{ \begin{matrix} V_{\ell m}(\beta,z)\ \bar{e}_{\ell m}(\beta,x) \\ I_{\ell m}(\beta,z)\ \bar{h}_{\ell m}(\beta,x) \end{matrix} \right\} e^{-j\beta y}\, d\beta \tag{2}$$

where the vector mode functions, $\bar{e}_{\ell m}$ and $\bar{h}_{\ell m}$, are given as

$$\begin{aligned} \bar{e}_{1m} &= \sqrt{\frac{\eta_{0m}}{2A}}\ \frac{1}{k_m} \left\{ -\hat{x}\ \gamma_m \cos \gamma_m(x+A) + \hat{y}\ j\beta \sin \gamma_m(x+A) \right\} \\ \bar{e}_{2m} &= \sqrt{\frac{\eta_{0m}}{2A}}\ \frac{1}{k_m} \left\{ \hat{x}\ j\ \beta \cos \gamma_m(x+A) - \hat{y}\ \gamma_m \sin \gamma_m(x+A) \right\} \end{aligned} \tag{3}$$

$$\begin{aligned} \bar{h}_{\ell m} &= \hat{z} \times \bar{e}_{\ell m} \\ k_m^2 &= \gamma_m^2 + \beta^2 \\ \gamma_m &= \frac{m\pi}{2A} \\ \eta_{0m} &= \begin{cases} 1 & m = 0 \\ 2 & m \geq 1 \end{cases} \\ \ell &= \begin{cases} 1 & \text{E-wave, } H_z \equiv 0 \\ 2 & \text{H-wave, } E_z \equiv 0 \end{cases} \end{aligned} \tag{4}$$

The modal voltages and currents are $V_{\ell m}(\beta,z)$ and $I_{\ell m}(\beta,z)$, and β and γ_m are the propagation constants in the y and x directions, respectively. Furthermore, the longitudinal components of the electric and magnetic fields are given as

$$E_z = \frac{1}{j\omega\varepsilon}\,\bar{\nabla}\cdot(\bar{H}_t \times \hat{z})$$
$$H_z = \frac{1}{j\omega\mu_0}\,\bar{\nabla}\cdot(\hat{z} \times \bar{E}_t) \tag{5a}$$

where ε is the permittivity in each region

$$\varepsilon = \begin{cases} \varepsilon_0 & s<z<s+h \quad \text{and} \\ & -b-t-d<z<-d-t \\ \varepsilon_{sr}\varepsilon_0 & 0<z<s \\ \varepsilon_{dr}\varepsilon_0 & -d<z<0 \\ \varepsilon_{tr}\varepsilon_0 & -t-d<z<-d \end{cases} \tag{5b}$$

The vector mode functions, $\bar{e}_{\ell m}(\beta,x)$ and $\bar{h}_{\ell m}(\beta,x)$, satisfy the orthonormality relations

$$\int_{-W}^{W} \bar{e}_{\ell m}\cdot\bar{e}^{*}_{\ell' m'}\,dx = \int_{-W}^{W} \bar{h}_{\ell m}\,\bar{h}^{*}_{\ell' m'}\,dx = \delta_{\ell\ell'}\delta_{mm'} \tag{6}$$

By substituting (1) and (3) into Maxwell's field equations and using (6), the transmission line equations for the modal voltages and currents are obtained

$$\frac{-dV_{\ell m}}{dz} = j\,\kappa_m\,Z_{\ell m}\,I_{\ell m}(z) \tag{7a}$$

$$\frac{-dI_{\ell m}}{dz} = j\,\kappa_m\,Y_{\ell m}\,V_{\ell m}(z)$$

where

$$\kappa_m = \sqrt{\omega^2 \mu_0 \varepsilon_0 - k_m^2} \qquad (7b)$$

$$Y_{\ell m} = 1/Z_{\ell m}$$

and

$$Z_{1m} = \frac{\kappa_{am}}{\omega \varepsilon_0} \qquad Z_{2m} = \frac{\omega \mu_0}{\kappa_{am}} \qquad \kappa_{am} = \sqrt{\omega^2 \varepsilon_0 \mu_0 - k_m^2}$$

for $-d-t-b \leq z \leq -d-t$

and $s \leq z \leq s+h$

$$Z_{1m} = \frac{\kappa_{sm}}{\omega \varepsilon_0 \varepsilon_{sr}} \qquad Z_{2m} = \frac{\omega \mu_0}{\kappa_{sm}} \qquad \kappa_{sm} = \sqrt{\omega^2 \varepsilon_{sr} \varepsilon_0 \mu_0 - k_m^2}$$

for $0 \leq z \leq s$

(7c)

$$Z_{1m} = \frac{\kappa_{dm}}{\omega \varepsilon_0 \varepsilon_{dr}} \qquad Z_{2m} = \frac{\omega \mu_0}{\kappa_{dm}} \qquad \kappa_{dm} = \sqrt{\omega^2 \varepsilon_{dr} \varepsilon_0 \mu_0 - k_m^2}$$

for $-d \leq z \leq 0$

$$Z_{1m} = \frac{\kappa_{tm}}{\omega \varepsilon_0 \varepsilon_{tr}} \qquad Z_{2m} = \frac{\omega \mu_0}{\kappa_{tm}} \qquad \kappa_{tm} = \sqrt{\omega^2 \varepsilon_{tr} \varepsilon_0 \mu_0 - k_m^2}$$

for $-d-s \leq z \leq -d$

With the transmission line equations in hand, they may now be solved in each of the five regions in terms of sine and cosine functions and arbitrary constants. The boundary conditions are such that the transverse electric and magnetic fields are continuous at z=s, z=-d, and z=-d-t. At z=0 the electric field is continuous for all x while the magnetic field is continuous only within the aperture. All of the above boundary conditions except those at z=0 may be used to eliminate constants in the general solutions of the transmission line equations. In order to use the conditions at z=0, additional orthonormality relationships are required. From (2) it can be shown that

$$\int_{-A}^{A} \bar{h}^{*}_{\ell',m'}(\beta,x) \cdot \hat{z} \times \bar{e}_{\ell m}(\beta,x)dx = \delta_{\ell\ell'}\delta_{mm'} \tag{8}$$

where δ_{xy} is the Kronecker delta. Using this along with (1), we obtain the modal voltage in the plane z=0 within the slot

$$V_{\ell m}(\beta,0) = \frac{1}{\sqrt{2\pi}} \int_{-A}^{A} dx' \int_{-\infty}^{\infty} dy' \, \bar{h}^{*}_{\ell m}(\beta,x') \cdot \hat{z} \times \bar{\varepsilon}_{t}(x',y') \, e^{j\beta y'} \tag{9}$$

where $\bar{\varepsilon}_{t}(x',y')$ is the transverse electric field in the plane z=0. These relationships are used along with the boundary conditions at z=0 to obtain the desired integral equation, given below in (10), for the longitudinal propagation constant β

$$\sum_{m=0}^{\infty} \int_{-W}^{W} [P_{1m}(\beta)\bar{h}_{1m}(\beta,x)\bar{h}^{*}_{1m}(\beta,x') + P_{2m}(\beta)\bar{h}_{2m}(\beta,x)\bar{h}^{*}_{2m}(\beta,x')] \cdot \bar{f}(x') \, dx' = 0 \tag{10a}$$

where

$$\bar{f}(x')\, e^{-j\beta y} = \hat{z} \times \bar{\varepsilon}_t(x',y') \tag{10b}$$

and

$$P_{1m} = \frac{k_0}{\kappa_{am}\tan(\kappa_{am}h)} \frac{1 - \frac{\varepsilon_{sr}\kappa_{am}}{\kappa_{sm}}\tan(\kappa_{am}h)\tan(\kappa_{sm}s)}{1 + \frac{\kappa_{sm}}{\varepsilon_{sr}\kappa_{am}}\frac{\tan(\kappa_{sm}s)}{\tan(\kappa_{am}h)}}$$

$$+ \frac{Q_{1m} - \frac{\varepsilon_{dr}k_0}{\kappa_{dm}}\tan(\kappa_{dm}d)}{1 + Q_{1m}\frac{\kappa_{dm}}{\varepsilon_{dr}k_0}\tan(\kappa_{dm}d)}$$

$$Q_{1m} = \frac{\varepsilon_{tr}k_0}{\kappa_{tm}} \cdot \frac{1 - \frac{\varepsilon_{tr}\kappa_{am}}{\kappa_{tm}}\tan(\kappa_{am}b)\tan(\kappa_{tm}t)}{\tan(\kappa_{tm}t) + \frac{\varepsilon_{tr}\kappa_{am}}{\kappa_{tm}}\tan(\kappa_{am}b)} \tag{11a}$$

$$P_{2m} = \frac{\kappa_{am}}{k_0\tan(\kappa_{am}h)} \frac{1 - \frac{\kappa_{sm}}{\kappa_{am}}\tan(\kappa_{am}h)\tan(\kappa_{sm}s)}{1 + \frac{\kappa_{am}}{\kappa_{sm}}\frac{\tan(\kappa_{sm}s)}{\tan(\kappa_{am}h)}}$$

$$+ \frac{Q_{2m} - \frac{\kappa_{dm}}{k_0}\tan(\kappa_{dm}d)}{1 + Q_{2m}\frac{k_0}{\kappa_{dm}}\tan(\kappa_{dm}d)}$$

$$Q_{2m} = \frac{\kappa_{tm}}{k_0} \frac{1 - \frac{\kappa_{tm}}{\kappa_{am}}\tan(\kappa_{am}b)\tan(\kappa_{tm}t)}{\tan(\kappa_{tm}t) + \frac{\kappa_{tm}}{\kappa_{am}}\tan(\kappa_{am}b)}$$

$$k_0 = \omega\sqrt{\mu_0\varepsilon_0} \tag{11b}$$

With the integral equation in hand, Galerkin's method is used to derive $\bar{f}(x)$, where $\bar{f}(x)$ is simply related to the slot electric field as previously defined in (10a). The vector function $\bar{f}(x)$ has x and y components which are expanded as follows

$$\begin{aligned} f_x(x') &= \sum_{n'=1}^{2N_x} a_{xn'} f_{xn'}(x') \\ f_y(x') &= \sum_{n'=1}^{2N_y} j\, a_{yn'} f_{yn'}(x') \end{aligned} \tag{12}$$

These equations are now substituted into (10). Next, the inner products of the result are taken with the functions

$$\hat{x}\, f_{xn}(x) \quad \text{and} \quad \hat{y}\, f_{yn}(x) \tag{13}$$

to obtain the following set of linear homogeneous equations in $a_{xn'}$, $a_{yn'}$, and β.

$$\sum_{n'=1}^{2N_x} a_{xn'} \left[\sum_{m=1}^{\infty} \frac{1}{Ak_m^2} \left\{ \beta^2 P_{1m}(\beta) + \gamma_m^2 P_{2m}(\beta) \right\} \tilde{f}_{xn} \tilde{f}_{xn'} \right]$$

$$+ \sum_{n'=1}^{2N_y} a_{yn'} \left[\sum_{m=1}^{\infty} \frac{1}{Ak_m^2} \beta\gamma_m \left\{ P_{2m}(\beta) - P_{1m}(\beta) \right\} \tilde{f}_{xn} \tilde{f}_{yn'} \right] = 0$$

$$n = 1, 2, \text{---}, 2N_x$$

$$\sum_{n'=1}^{2N_x} a_{xn'} \left[\sum_{m=1}^{\infty} \frac{1}{Ak_m^2} \beta\gamma_m \left\{ P_{2m}(\beta) - P_{1m}(\beta) \right\} \tilde{f}_{yn} \tilde{f}_{xn'} \right]$$

$$+ \sum_{n'=1}^{2N_y} a_{yn'} \left[\sum_{m=0}^{\infty} \frac{\eta_{0m}}{2Ak_m^2} \left\{ \gamma_m^2 P_{1m}(\beta) + \beta^2 P_{2m}(\beta) \right\} \tilde{f}_{yn} \tilde{f}_{yn'} \right] = 0 \qquad (14)$$

$$n = 1, 2, \text{---}, 2N_y$$

where

$$\tilde{f}_{xn} = \int_{-W}^{W} \sin \gamma_m(x' + A) \; f_{xn}(x') \, dx'$$

$$\tilde{f}_{yn} = \int_{-W}^{W} \cos \gamma_m(x' + A) \; f_{yn}(x') \, dx' \qquad (15)$$

If (14) is to yield nontrivial solutions, the determinant of the coefficient matrix must be zero. From this, the propagation constant, β, may be evaluated.

Now that we have a set of equations to solve, we can find β. The next step is to choose a set of basis functions, which must satisfy several properties. They must account for the edge effect, they must give an increasingly more accurate solution of the aperture fields with an increased number of terms in the series, and they must allow an analytical integration in (15). With these criteria in mind, the basis functions were chosen as

$$f_{xm} = U_n\left(\frac{x}{W}\right)$$

$$f_{yn} = \frac{T_{n-1}}{\sqrt{1 - \left(\frac{x}{W}\right)^2}} \tag{16}$$

where $T_n(z)$ and $U_n(z)$ are Chebyshev polynomials of the first and second kinds, respectively. After substituting these equations into (13) and (14), asymptotic approximations are made for large m. The determinantal equation is now solved and the longitudinal propagation constant, β, is calculated. Some numerical results are given in the next section.

Now that the propagation constant has been calculated, the next step is to calculate the characteristic impedance of the fin line. Since this is a quantity that is defined rigorously only for TEM waves, several different definitions are possible. The definition chosen was

$$Z_c = \frac{V_x^2}{2P} \tag{17}$$

where V_x is the voltage between the fins at a given point on the line, and P is the total power traversing the cross section of the line at that point. For other possible definitions see reference [2].

Numerical Results

Before making any calculations, it was necessary to determine the number of expansion functions needed to obtain sufficient accuracy in the final result. In order to make this determination, the dispersion constant and normalized characteristic impedance were calculated for the structure

shown in Figure 1 at 100 GHz. This case represents the most severe convergence case of all those presented here because it has the highest frequency, the largest slot width, and the lowest substrate dielectric constant. Convergence is shown by increasing the values of N_x and N_y, the number of terms in the expansion. The results for the normalized propagation constant and characteristic impedance are shown in Table 1 as a function of N_x and N_y. The data show that solutions for $N_x=N_y=2$ yield an accuracy to three decimal places. Since this was considered sufficient, all calculations presented here use these values.

The results of the calculations are now presented. Figures 2a and 2b show the dispersion characteristic and characteristic impedance of the configuration shown in Figure 1. The dispersion characteristic was calculated for the first four modes of the given structure, and the impedance was calculated for the first two even modes. Note that the range of single-mode operation of this fin line is larger than that for the WR-19 metal waveguide. For the fin line, this bandwidth is about 35.0 GHz, while that for the WR-19 metal waveguide is 31.4 GHz.

The effect of varying the width of the slot is shown in Figure 3. As the slot width decreases, the cutoff frequencies of the first and second even modes decrease.

Figure 4 shows the effect of varying the substrate dielectric constant on the dispersion characteristics of the first and second even modes. Here, W/A = 0.2 and dispersion characteristics for the first and second even modes are presented for ϵ_r = 2.2, 3.8, and 9.6.

Finally, in Figures 5a and 5b, a comparison is made between our data and Knoor and Shayda's. The configuration is exactly that of Figure 3 in this

TABLE 1

CONVERGENCE TEST CALCULATIONS FOR THE CONFIGURATION IN FIGURE 1 AT 100 GHZ

		First Even Mode		Second Even Mode	
N_x	N_y	ε_{eff}	z_c	ε_{eff}	z_c
0	1	1.071	1.204	0.381	0.768
1	1	1.074	1.223	0.381	0.766
1	2	1.064	1.185	0.381	0.766
2	2	1.064	1.185	0.381	0.766
2	3	1.064	1.185	0.381	0.766
3	3	1.064	1.185	0.381	0.766

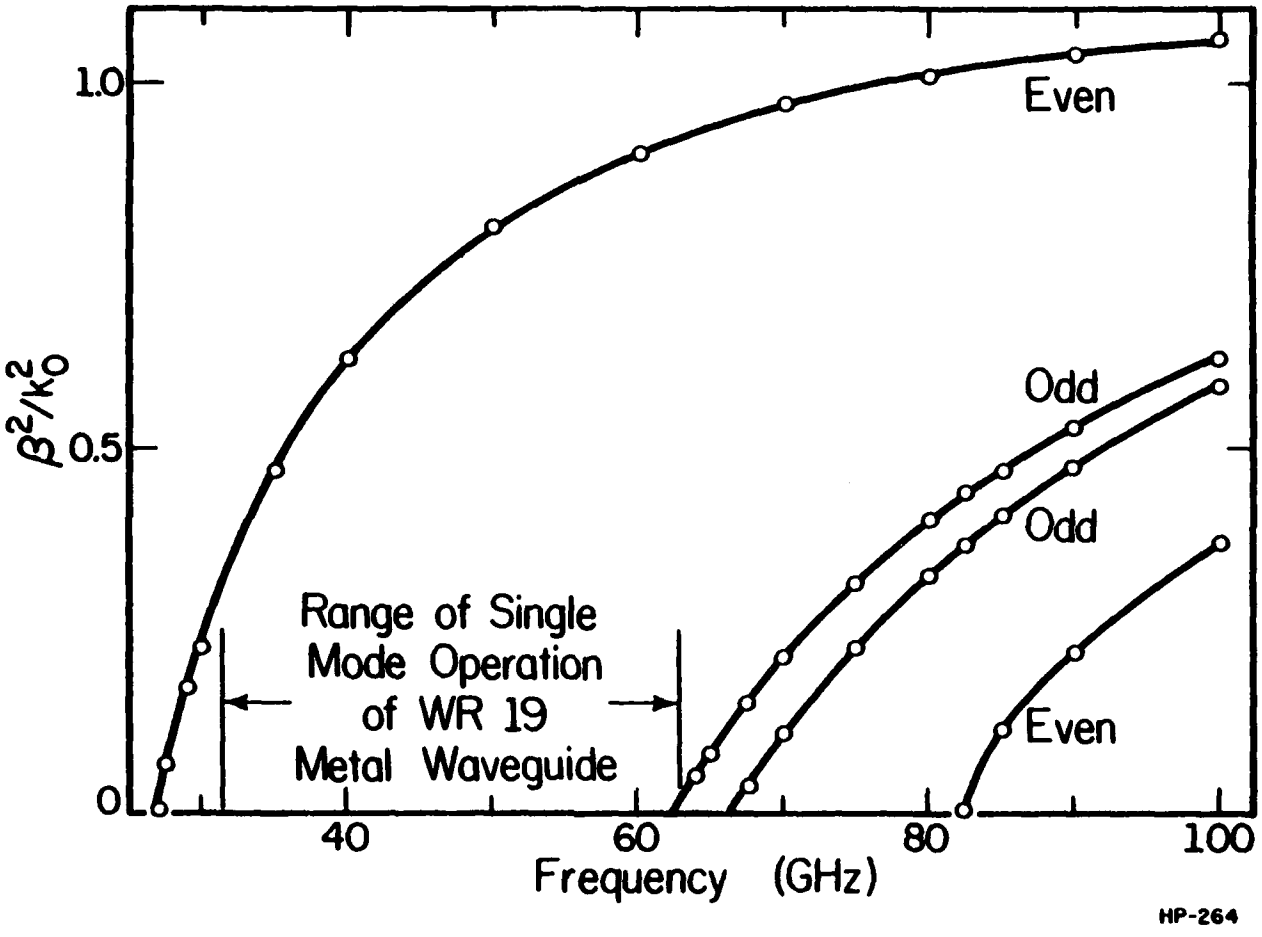

Figure 2.

Figure 2a: Normalized propagation constant of the first four modes of the configuration in Figure 1. The arrow represents the range of single-mode operation of the WR-19 metal waveguide. Note the wider bandwidth of the fin line.

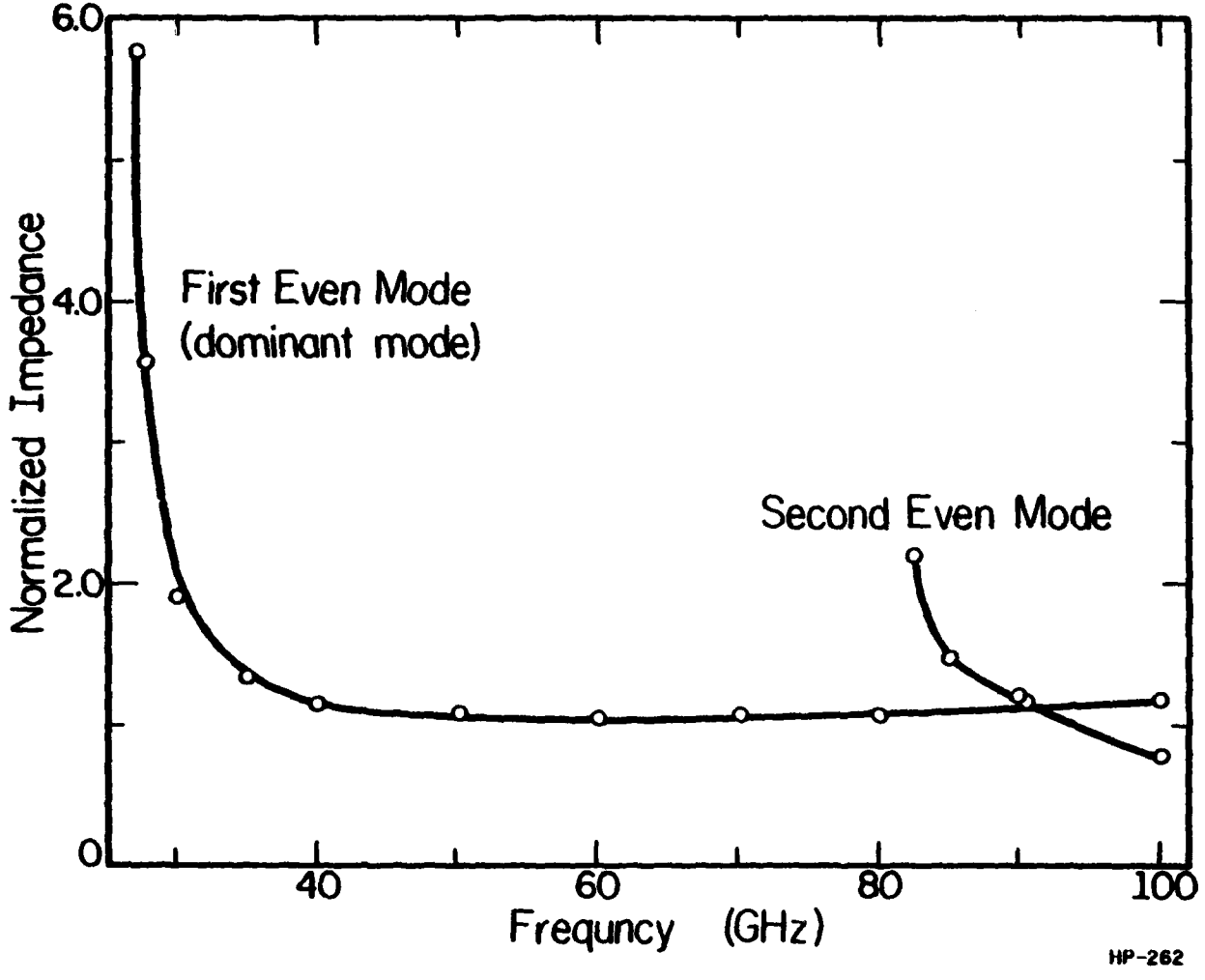

Figure 2b. The normalized characteristic impedance of the first two even modes for the same configuration.

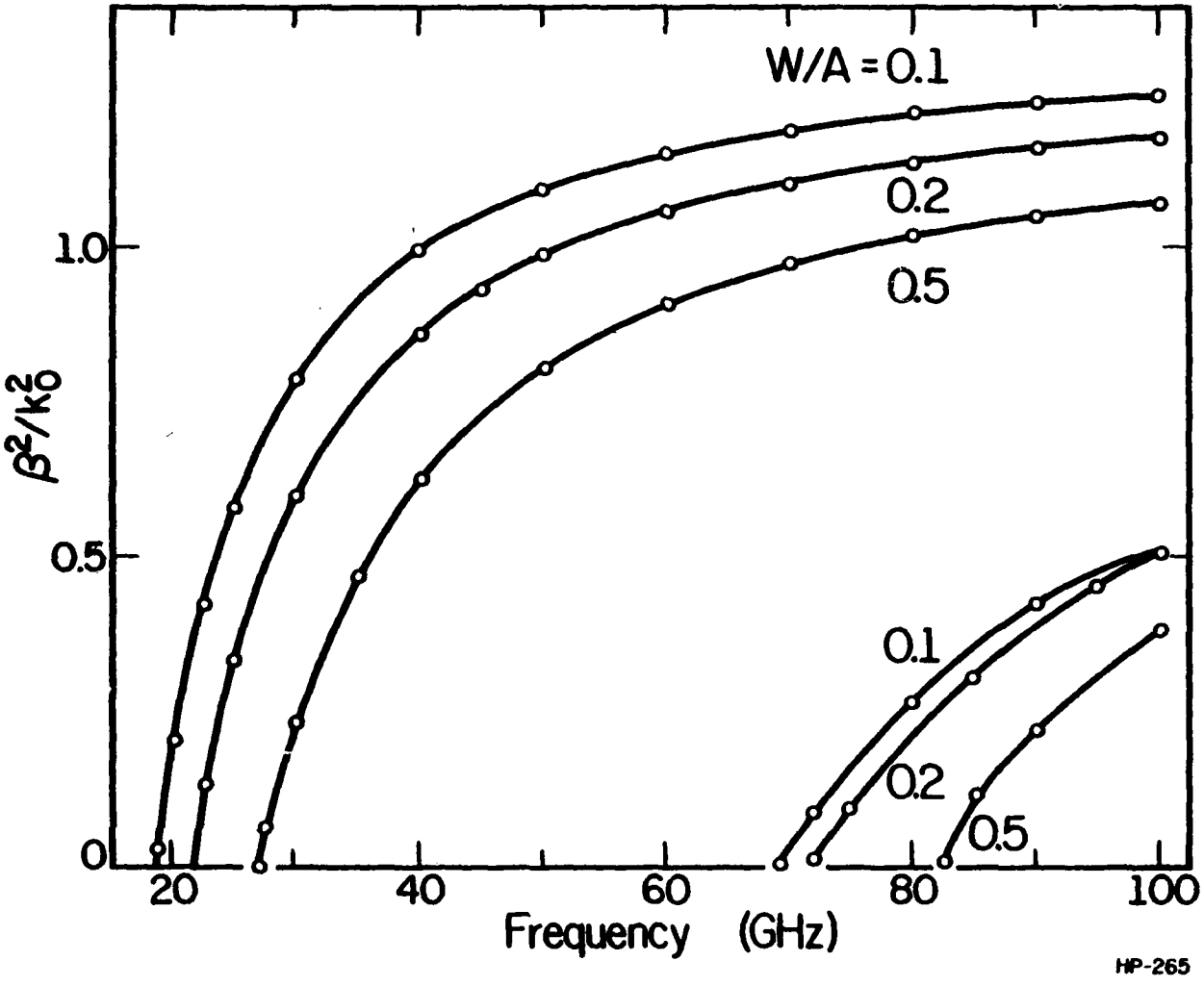

Figure 3. The effect of varying the slot width on the dispersion characteristics of the first two even modes.

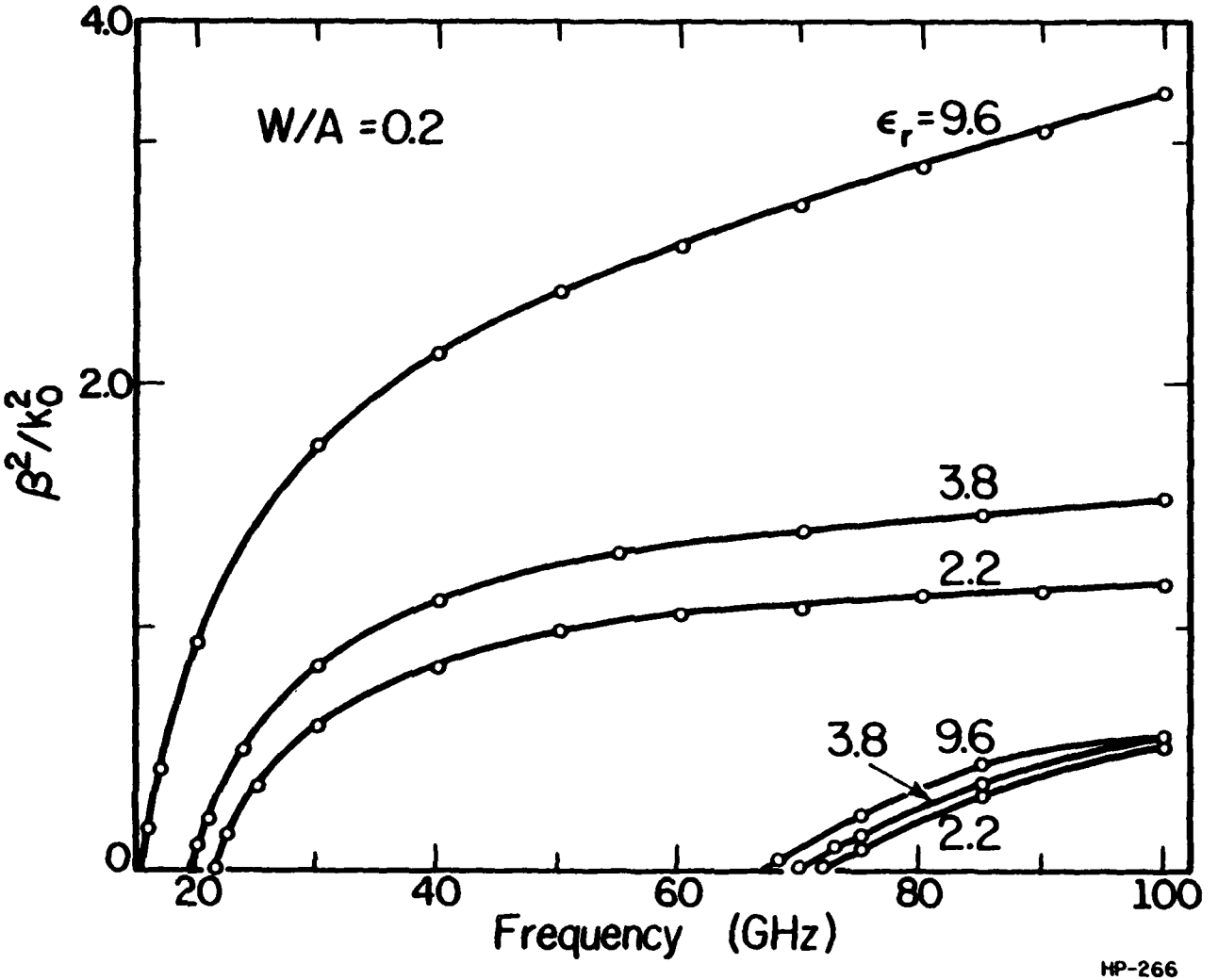

Figure 4. The effect of varying the substrate dielectric constant on the dispersion characteristics of the first two even modes. Here, the slot width is such that W/a = 0.2.

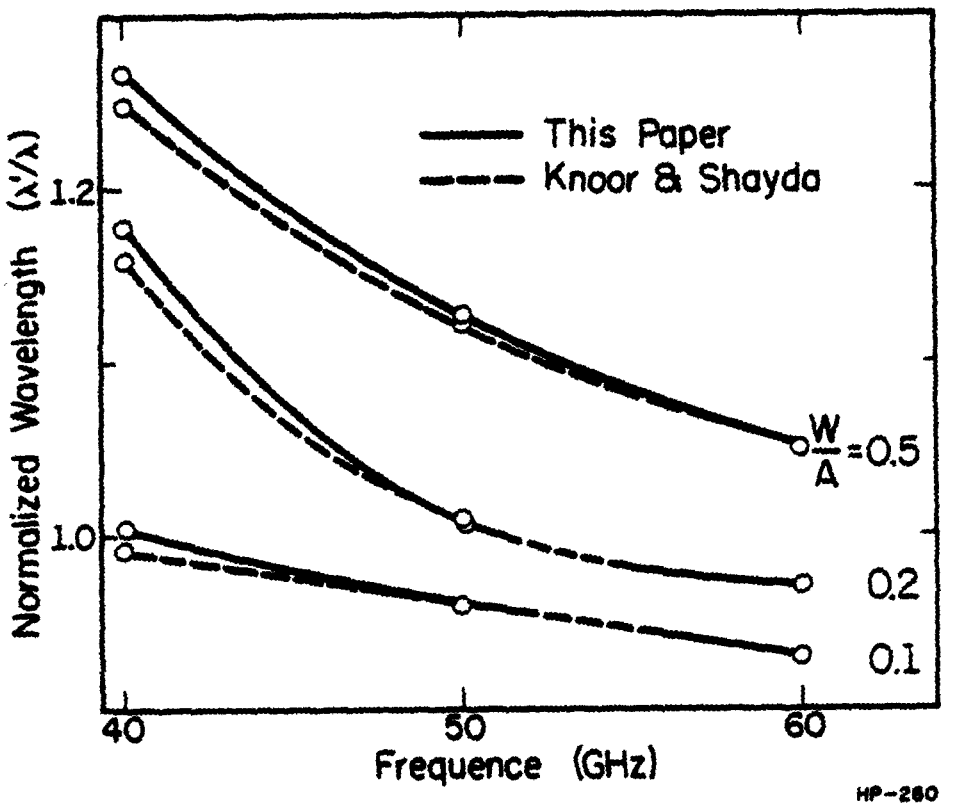

Figure 5.

Comparison of our data in Figure 3 to Knoor and Shayda's data in Figure 8 of reference [1].

Figure 5a is the normalized wavelength

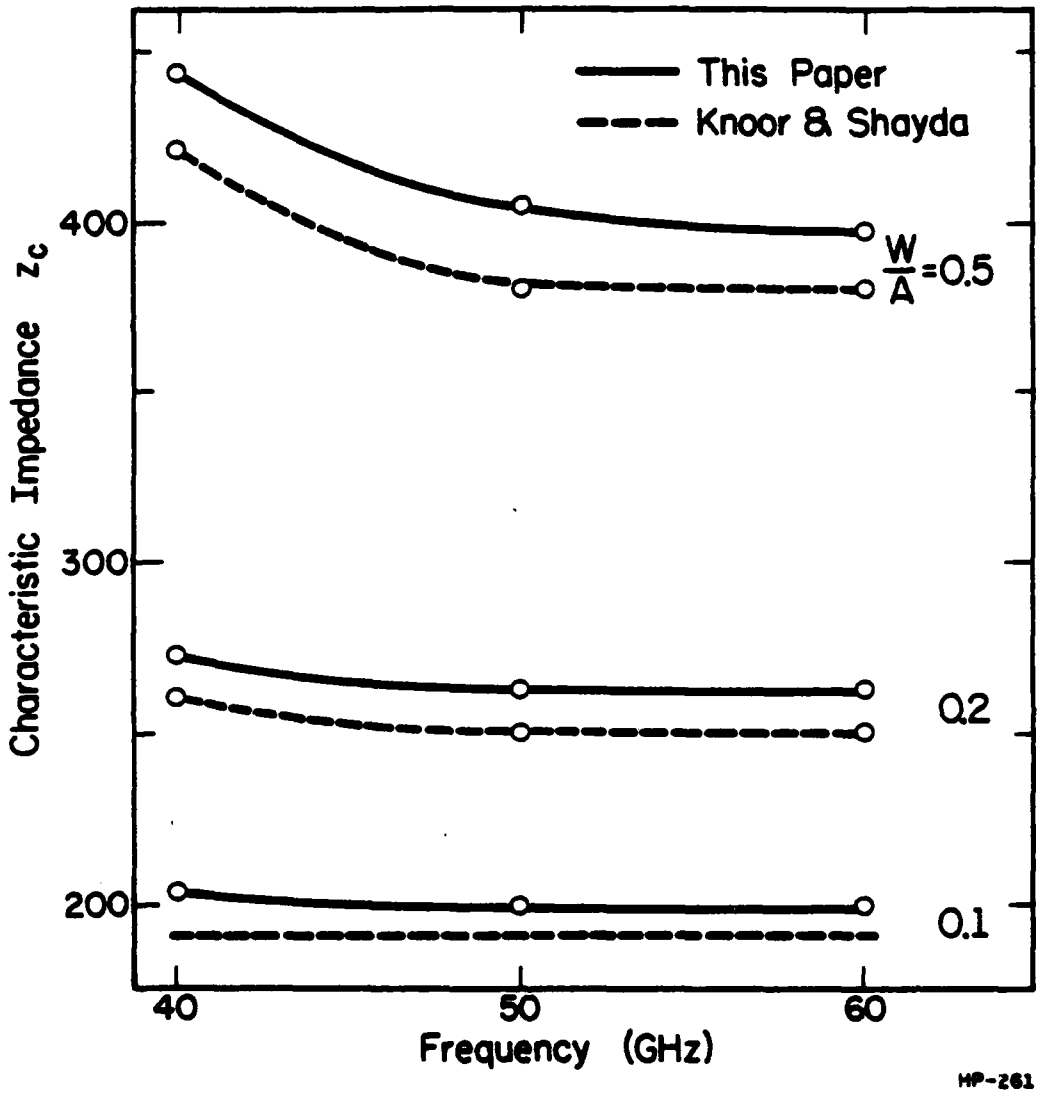

Figure 5b is the characteristic impedance.

paper, and Figure 8 in reference [4]. There is a maximum difference of about 2% for the normalized wavelength, and about 6% for the characteristic impedance. We believe our results to be more accurate for the following reason. Our calculations were made with N_x and N_y both equal to two, whereas Knoor and Shayda had N_x equal to zero and N_y equal to one. It is expected that a higher number of basis functions should yield a more accurate solution.

Conclusions

In this paper, a unilateral fin line on a dielectric substrate has been analyzed using the network analysis method of electromagnetic fields. Results for higher-order modes have been obtained as well as for dominant modes, and the results are believed to be more accurate than those previously obtained since the aperture fields are calculated exactly. Furthermore, it has been shown that the range of single-mode operation is greater for the fin line analyzed than that for the WR-19 metal waveguide. This property of the fin line tends to make it appear even more attractive for millimeter-wave circuit applications than previously thought.

References

1. J. Knoor and P. Shayda, "Millimeter-wave fin-line characteristics," IEEE Trans. Microwave Theory and Tech., vol. MTT-28, pp. 737-743, July 1980.

2. T. Itoh and R. Mittra, "Dispersion characteristics of slot lines," Elec. Lett., vol. 7, pp. 364-365, July 1971.

3. L. Schmidt and T. Itoh, "Spectral analysis of dominant and higher order modes in fin lines," IEEE Trans. Microwave Theory and Tech., vol. MTT-28, pp. 981-985, September 1980.

4. T. Kitazawa et al., "Analysis of the dispersion characteristic of slot line with thick metal coating," IEEE Trans. Microwave Theory and Tech., vol. MTT-28, pp. 387-392, April 1980.


TE
MED
8